

## Research Article

# Electrochemical Studies of WC-Flyash HVOF Coating Interface on SA209-T1 Steel under 3.5 NaCl Solution

D. Elango,<sup>1</sup> A. Daniel Das ,<sup>2</sup> S. P. Kumaresh Babu,<sup>3</sup> S. Natarajan,<sup>3</sup> and A. Yeshitla <sup>4</sup>

<sup>1</sup>Department of Metallurgical and Materials Engineering, National Institute of Technology, Tiruchirappalli, Tamil Nadu, India

<sup>2</sup>Department of Mechanical Engineering, Karpagam Academy of Higher Education, Coimbatore, Tamilnadu, India

<sup>3</sup>Department of Metallurgical and Materials Engineering, National Institute of Technology, Tiruchirappalli, Tamil Nadu, India

<sup>4</sup>Department of Biotechnology College of Biological and Chemical Engineering, Addis Ababa Science and Technology University, Addis Ababa, Ethiopia

Correspondence should be addressed to A. Yeshitla; [alazar.yeshi@aastu.edu.et](mailto:alazar.yeshi@aastu.edu.et)

Received 15 July 2021; Revised 10 August 2021; Accepted 20 October 2021; Published 9 November 2021

Academic Editor: Samson Jerold Samuel Chelladurai

Copyright © 2021 D. Elango et al. This is an open access article distributed under the Creative Commons Attribution License, which permits unrestricted use, distribution, and reproduction in any medium, provided the original work is properly cited.

In this present research, the coatings of SA209-T1 using high velocity oxygen fuel were employed for the application of boiler tubes. Due to the adaptation of corrosion easy in boiler material, the research of those properties is significant because of its criticality and functionality during the service time. A right coating was found and applied on the SA209-T1 surface against corrosive environments. Good corrosion resistance is achieved by WC-flyash coatings applied on SA209-T1 substrate. The 90% WC-10% flyash coatings were found to be more protective followed by SA209-T1 steel. WC-flyash covering was tracked down so that the covering is compelling to secure the SA209-T1 steel substrate. It is reasoned that the arrangement of NiO, Cr<sub>2</sub>O<sub>3</sub>, CoO, and NiCr<sub>2</sub>O<sub>4</sub> could add to the advancement of consumption opposition in coatings. The steel of uncoated endured erosion as extraordinary stripping and spalling of the scale, which could be because of the development of Fe<sub>2</sub>O<sub>3</sub> oxide scale unprotectively. This paper reveals the performance, applications, and development of 90wt.% WC and 10wt.% fly ash through HVOF coating in SA209-T1 for electrochemical corrosion studies at room temperature.

## 1. Introduction

HVOF showering is applied predominantly to metallic and cermet coatings due to the dissolving force of the HVOF splashing weapons and frameworks. Notwithstanding, because of the greater kinetic energy, more limited stay reason of particles in the fire, and lower fire temperature contrasted with the plasma splash, HVOF offers an intriguing mix to create thick coatings with controlled stage changes. For WC-Co-based material, it is noted that during the time of flight, showered particles soften to various degrees relying upon their density, size, and dwell time. Liquid Co breaks down the WC grains through carbon misfortune that happens by dissemination through the fluid followed by the response of oxygen to environmental factors. There can be a lot of carbon and tungsten broke down from the framework material, particularly from the external area of splashed particles. During the cooling time, Co-

rich liquid becomes supersaturated coming about because of the development of W<sub>2</sub>C and other blended carbides. Substantial cooling rates can even be liable for the development of the formless/nanocrystalline network stage. At the time of cooling, precipitation of blended carbides, like the estimated time of arrival, carbide stage may happen in the co-rich material. These impacts are generally noticeable on the external center of the particles. In the little size particles, the entire molecule can be impacted by decarburization. On the chance that cooling is sufficiently quick, the lattice will remain indistinct and super-saturated with C and W. At the point when heat treatment of the coating occurs, the precipitation of the estimated time of arrival begins at a temperature of over 600°C bringing about the checked increment of hardness and a decrease in lingering stresses in the covering [1–3]. The erosion was characterized by Rapp and Zhang as the speed up of the oxidation of the material by temperature raise, prompted by a meager film of melded salt

stores [1]. The reasons for the disappointment of heater tube due to the fireside consumption in waste warmth recuperation evaporator using fumes of gas turbine terminated with fast diesel were investigated by Srikanth et al. [2]. Moreover, they revealed that the consumption happens on account of the response of sulfur species in the gas stage to the surface of the metals. The presence of sulfur in coal and fuel oils yielded  $\text{SO}_2$  during ignition which might be a part of this way oxidized to  $\text{SO}_3$ . The NaCl responds to  $\text{SO}_3$  and fume when burning temperature yields  $\text{Na}_2\text{SO}_4$ . Limited number of vanadium might be likewise has been available in oils which are ignition structures  $\text{V}_2\text{O}_5$ . This could additionally respond to  $\text{Na}_2\text{SO}_4$  low frame liquefying sodium vanadate, which is very destructive to substantial material temperature utilized in the burning framework [3, 4]. Evaporator prepared cannot meet the prerequisite for both high thermal consumption obstruction and high thermal strength. Covering gives a method of broadening the constraints of utilization of materials under good finish because of their presentation ability, through permitting the good mechanical strength of substrate metals to be kept while securing it against erosion and wear [5]. Nickel chromium compound has been utilized as a covering to manage oxidizing conditions at high temperature. At the point when nickel and chromium are alloyed, the component oxidizes  $\text{Cr}_2\text{O}_3$ , which may make it reasonable for use up to around  $1200^\circ\text{C}$ . Nonetheless, its utilisation is restricted to temperatures under  $800^\circ\text{C}$  [6]. The warm splashed 50/50 nickel chromium composite is typically suggested as disintegration erosion insurance for heater tube in power age application [7]. Chuanxian et al. [8] and Lio et al. [9] have announced wide utilization of cermet warm splash coatings in clear circumstances since they consolidate a few benefits like protection from scraped area, high temperature, disintegration, and destructive airs. The HVOF measure is accounted for an adaptable innovation, and it is embraced by numerous enterprises because of its adaptability, cost adequacy, and predominant nature of covering created. The hypersonic speed of the fire abbreviates the hour of cooperation between the fire and powder, and less temperature of fire restricts the deterioration and grain development of coatings. Because of the great effect speed of particles, the covering shows a uniform microstructure, substantial cement strength, high thickness, low porosity, and substantial firm strength of separate splats [10]. The ultimate target of the current research is to describe the substantial temperature erosion systems for high velocity oxy fuel metallic coatings on heater steel to be specific ASTM SA 209-T1 grade Al in a forceful climate of liquid salt ( $\text{Na}_2\text{SO}_4$ -60% $\text{V}_2\text{O}_5$ ). SEM/EDAX, XRD, and EPMA methods have been utilized to describe consumption items after hot erosion under cyclic conditions at  $900^\circ\text{C}$ .

## 2. Investigation of Experiment

**2.1. Materials and Methods.** The boiler tube steel with ASTM SA209-T1 grade Al (GrAl) compound structure as demonstrated in Table 1 has been utilized under the substrate steel. In north India, some power plants have utilized this

material as evaporator tube material. The steel tests were sliced to shape around  $20\text{ mm} \times 20\text{ mm}$  measured samples. The samples were neatly cleaned and grit blasted with  $\text{Al}_2\text{O}_3$  (coarseness 45) preceding use of the high velocity oxy fuel shower coatings. The examination has been performed for coated and uncoated specimens with the end goal of correlation [9]. The uncoated specimen was reflecting cleaned to one  $\mu\text{m}$  of alumina wheel fabric cleaning before erosion examination. The outside of the consumed workpieces was outwardly seen to record tone, stripping, and spalling of scale during electrochemical erosion. The specimen after erosion run has been analyzed by SEM analysis.

**2.2. Thickness of Coverings.** The covering thickness was measured through the BSE images which was normally around  $300\mu\text{m}$ . The deliberate estimations of the porosity for a splashed covering are shown in Table 2. The spray variables used during HVOF showering are shown in Table 3.

**2.3. Specimens Arrangement for Corrosion.** The hacksaw was used to cut the coated interface, and rough sheets were used for deburring the specimens. The parent metal was additionally ready for examination to connect the erosion conduct with the WC-flyash covered specimens [11]. The SiC 1200 grade emery paper having rough coarseness is used for setting up the surface of the metal, and refined water is used to clean the specimen and then dried at room temperature.

**2.4. Electrochemical Studies.** Figure 1 shows the Autolab electrochemical workstation; the consumption opposition is examined by the utilization of potentio-dynamic polarizing bends and electrochemical impedance spectroscopy at  $28^\circ\text{C}$  of ambient temperature. The examinations have been conducted through utilizing Autolab instruments, CECRI, Karaikudi, Tamil Nadu, India, with polarization forecast programming. Saturated calomel anode and platinum were used as cathode. On a superficial level zone, the examination has been performed for  $2\text{ cm}^2$  for every single time. At a time frame  $\text{mV}-1.500\text{ mV}$ , the curves of polarisation were estimated at a pace of scan of  $\text{mV/s}$ . A specimen of WC-flyash covered at OCP for sixty minutes was held with electrochemical impedances [3].

**2.5. Surface Morphology Analysis by SEM and EDS.** A cold cathode Hitachi S 4800 field electron SEM lens is utilized to identify the morphology of the surface. The thermo NORAN NSS power scatter X-beam (EDS) is matched with the field electron SEM which gave a best-in-class imaging gadget of value around  $1\text{ nm}$  in goal at  $15\text{ kV}$  of beam power. The component appropriation could be described utilizing EDS investigation. The yttrium aluminum garnet backscattered electron identifier is accessible alongside field electron SEM and is utilized to catch the contrast improved pictures of multistage materials [4].

TABLE 1: SA209-T1 chemical composition (OES method).

Elements	Mn	C	P	Si	S	Mo	Fe
Weight %	0.45	0.19	0.025	0.34	0.024	0.55	Balance

TABLE 2: Thickness of scale (average) and porosity of coverings.

Sl. no.	Depletion	$K_p$ ( $10^{-10} \text{g}^2 \cdot \text{cm}^{-4} \cdot \text{s}^{-1}$ )	Thickness of scale (average) ( $\mu\text{m}$ )	Porosity (%)
1	Uncovered SA209-T1	6860.8	950	—
2	WC-flyash-coated	1515.3	850	1.35–1.5

TABLE 3: Spray variables utilized during HVOF showering.

Sl. no.	Spray variables	Hipojet-209-T10
1	Flow rate of oxygen	225 LPM
2	Flow rate of fuel (LPG)	65 LPM
3	Flow rate of air	6100 LPM
4	Diameter of wire/size of the particle	$-30 + 15 \mu\text{m}$
5	Wire/powder feed	30 g/min
6	Spray distance	200 mm

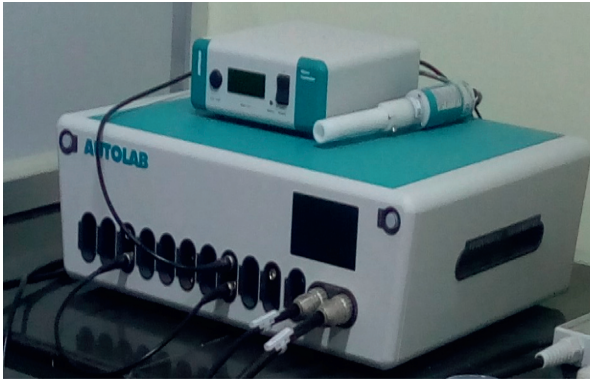


FIGURE 1: Electrochemical workstation to identify the utilization of potentiodynamic polarizing bends and electrochemical impedance spectroscopy.

2.6. *Optical Microscope.* Perception of the grain design of base materials and covering interface is performed by cutting-edge mechanical sorting on a large scale. It is likewise used to quantify the normal covering thickness statement utilizing direct block attempt strategy.

### 3. Discussion of Results

3.1. *EDS-Based Morphological Study.* The surface morphology of the coated and uncoated prepared after cyclic hot erosion was shown by the SEM images and is shown in Figure 2.  $\text{Fe}_2\text{O}_3$  could be the dominating stage which demonstrates the uncoated steel by EDAX investigation. EDAX examination of size of WC-flyash covered example showed little amounts of  $\text{Cr}_2\text{O}_3$  and  $\text{Fe}_2\text{O}_3$  presence alongside largest level of NiO (96%). The coated specimen size has high level of NiO and  $\text{Cr}_2\text{O}_3$  alongside other minor stages MnO,  $\text{Fe}_2\text{O}_3$ ,  $\text{SiO}_2$ , and so on. The EDAX of the WC flyash coated steel scale showed CoO,  $\text{Fe}_2\text{O}_3$  with an exceptionally small amount of  $\text{WO}_3$ . The size of coated steel

stellite-6 shows the predominance of CoO alongside  $\text{Cr}_2\text{O}_3$  and  $\text{Fe}_2\text{O}_3$ .

Figure 3 shows the WC-flyash-coated steel EPMA planing analysis; it shows that the substrate diffuses Fe in to coatings whereas Si and Mn concentrated at the substrate and coating interface. Throughout the scale, Cr and Ni are present. Also, the coating shows the Ni-rich pockets. The nickel (Ni) rich region depletes the chromium (Cr) region. The uncoated steel EPMA mapping of scale shows Co-rich layer in the scale top and contains chromium. The presence of the tungsten-rich streaks was also seen in the scale. Si is precipitated out to the substrate boundary [12–15]. Whereas EPMA mapping for uncovered steel. Figure 4 shows that top layer to be Cr rich and below that presence of Ni in higher concentration. Notification of iron migration from the substrate to the top layer of the scale. The oxide scale mainly consisted of  $\text{Fe}_2\text{O}_3$  has been indicated by WC-flyash-coated steel EPMA map. Fe has been diffused from substrate into the coating for all [16, 17].

3.2. *Optical Microscopic Studies.* By analyzing the proof of micrographs of the coating obtained by HVOF, the coatings deposited on GrA1 steel substrates shown in Figure 5 also show uniform thickness,  $103 \pm 6 \mu\text{m}$ , as well as good adhesion to the substrate.

3.3. *Potential Dynamic Polarization Studies.* The unique polarization is performed for uncoated steel at 28 °C room temperature as per ASTM G59-97(2020) standards. The checking of polarization at the rates between  $0.01 \text{mVs}^{-1}$  to  $50 \text{mVs}^{-1}$  and plotting of chart are shown in Figure 6. The outcome is derived from three separate sources: the uncoated base material, the WC-flyash-coated base material, and the interface. The run of the mill anodic terminal polarization conduct of SA209-T1 in NaCl arrangement comprises of dynamic disintegration, lack of involvement, and abrupt addition in the thickness of the current due to the pitting on the base material. Due to this abrupt augmentation of thickness of the current, the pitting is steady. The covered and uncoated examples are likewise tried at greatest output rate, neglected to show a stable pitting. Due to this reason, the  $\text{Cr}_2\text{O}_3$  is present in the coated specimens [18–20]. The uncoated locales are the most noteworthy consumption district as opposed to the interface area of the WC-flyash covered SA209-T1 steel concentrate through polarization bends. The degree of pitting at the uncoated is too poor contrasted with the WC-flyash covered SA209-T1 steel.

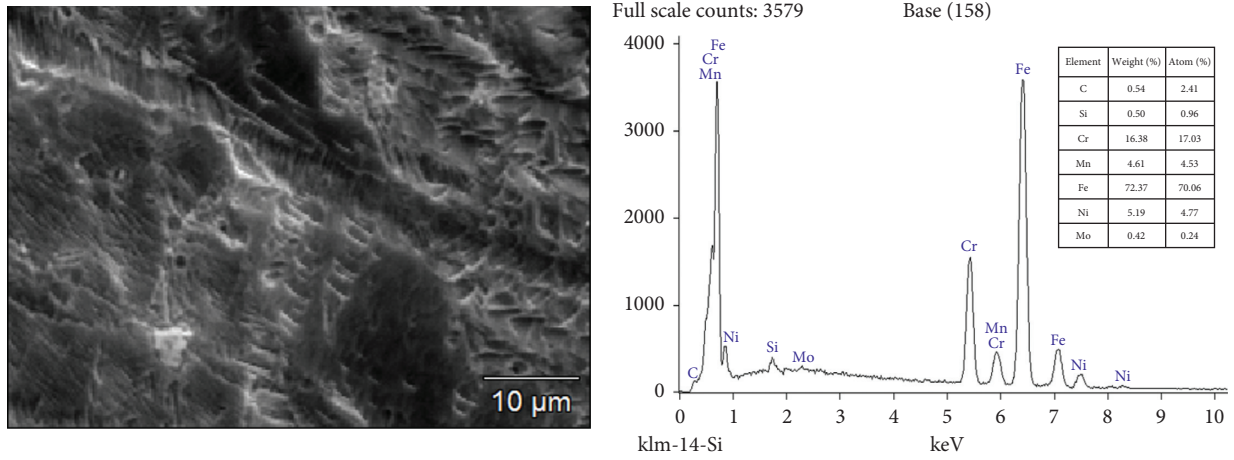


FIGURE 2: EDS and SEM investigation of the good material at dendritic multiperiod of 100 microns.

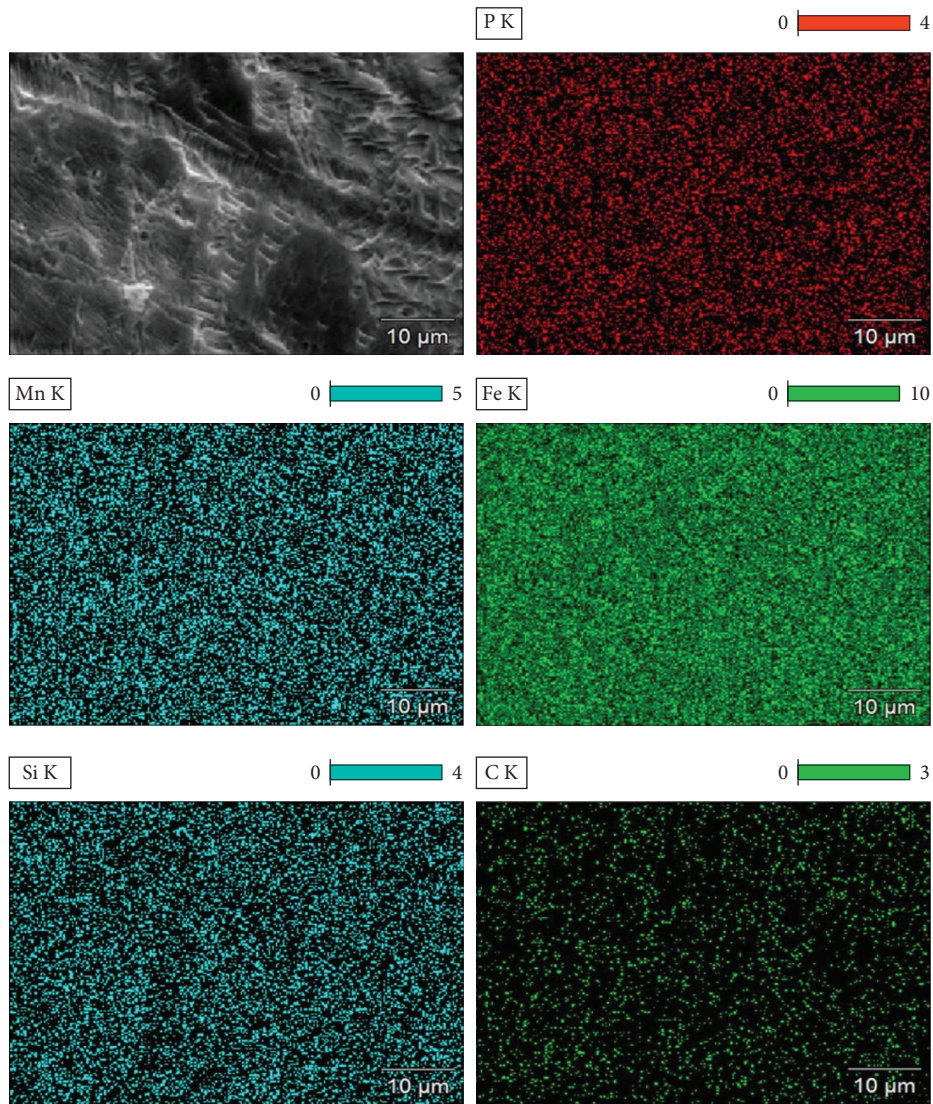


FIGURE 3: Arrangement picture BSEI and X-ray mapping of the cross segmentation of WC-flyash-covered GrA1 steel exposed to electrochemical consumption under 3.5%NaCl solution.

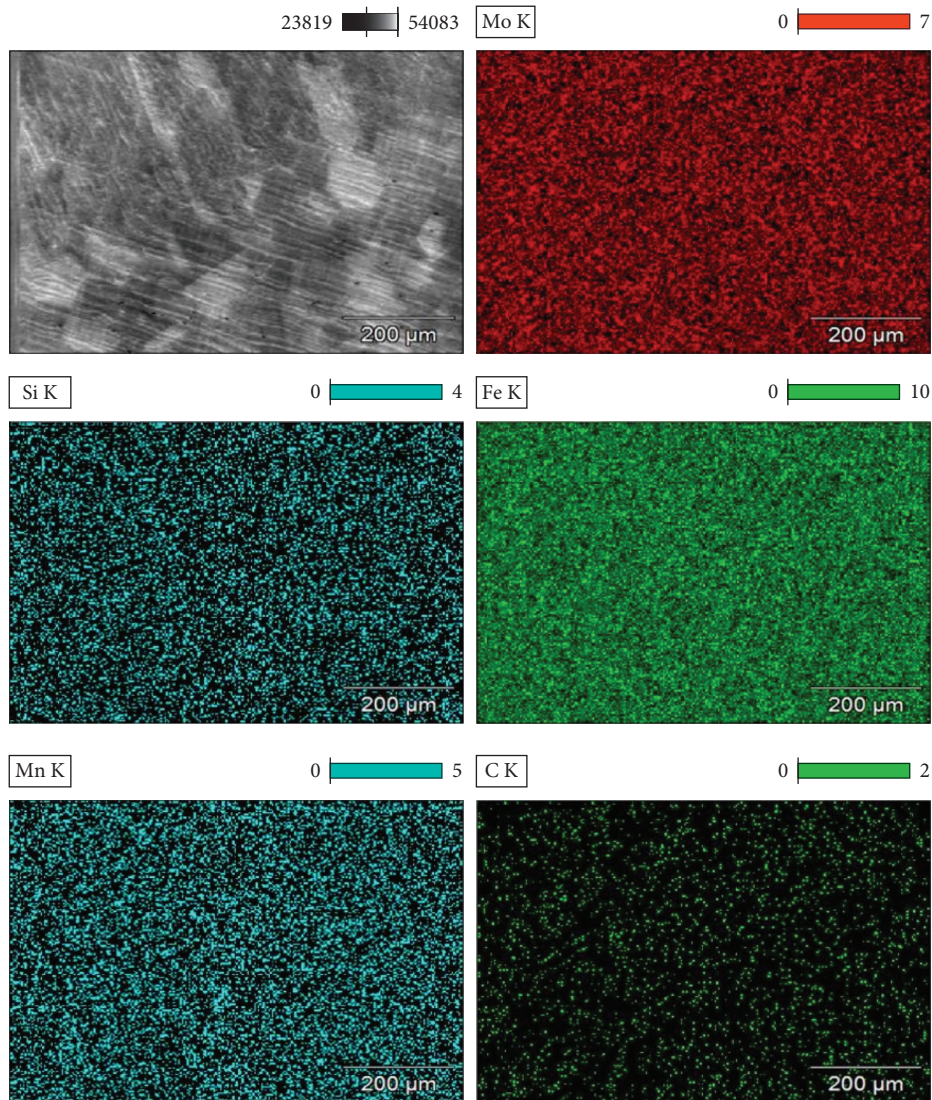


FIGURE 4: Arrangement picture BSEI and X-ray mapping of the cross portion of uncoated GrA1 steel exposed to electrochemical consumption under 3.5%NaCl solution.

**3.4. Electrochemical Impedance Spectra.** Affirmations of defensive film development on the surface of the metal, AC spectra (electro substance impedance range) have been utilized as per ASTM G106 standards. The obstruction of charge move ( $R_t$ ) increments when the defensive film structures on the surface of the metal; the capacitance esteem diminishes with the twofold level. Variables of the AC impedance incorporate burden transmission obstruction ( $R_t$ ) and twofold layer capacitance ( $CdL$ ) from Nyquist plots of base metal (B), combination zone (F), and the influenced region (D), as demonstrated in Figure 7. The figure curves of EIS show that there is serious erosion happened on the zone of warmth influencing and base material and the combined zone [21]. WC-flyash covered GrA1 steel has better destructive obstruction, and uncoated has helpless destructive opposition. The genuine impedance segment ( $Z'$ ) speeds up to the greatest degree in the interface with varieties of the qualities at the primary

phase of erosion. Subsequently, compared with the uncoated and WC-flyash covered GrA1 steel climate, the warmth affecting climate's consumption power is low [22–24].

EIS was utilized to research the erosion insurance for the steel. Figure 7 shows the Nyquist plots and Bode plots recorded for the WC-flyash-covered GrA1 steel. As shown in Figure 7, the measurement of the crescent in the Nyquist circle of the example with in various environments is bigger than that of the covered GrA1 steel, demonstrating that the tempering interaction has upgraded the consumption obstruction. The biggest crescent breadth was noticed, for example, WC-flyash covered GrA1 steel, which affirms its best consumption hindrance execution among all specimens [25–27].

Figure 8 shows the phase angle plots of uncoated GrA1, interface, and WC-flyash-coated GrA1 steel. Another time steady was seen in the low recurrence area, and the first one was moved to a higher recurrence locale.

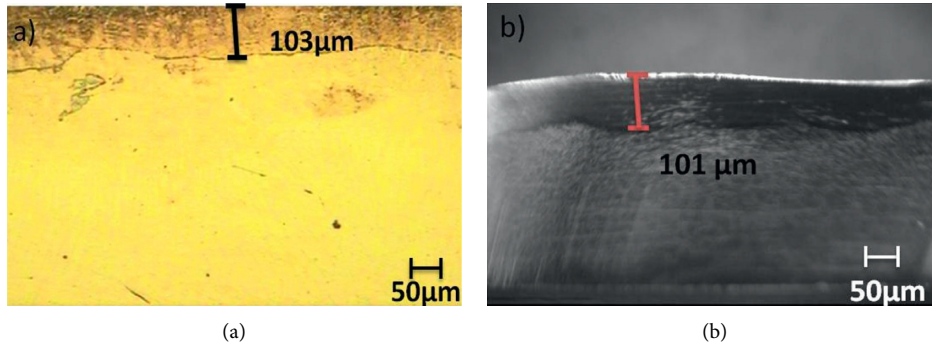


FIGURE 5: Micrographs of the coatings obtained by HVOF (a) and (b).

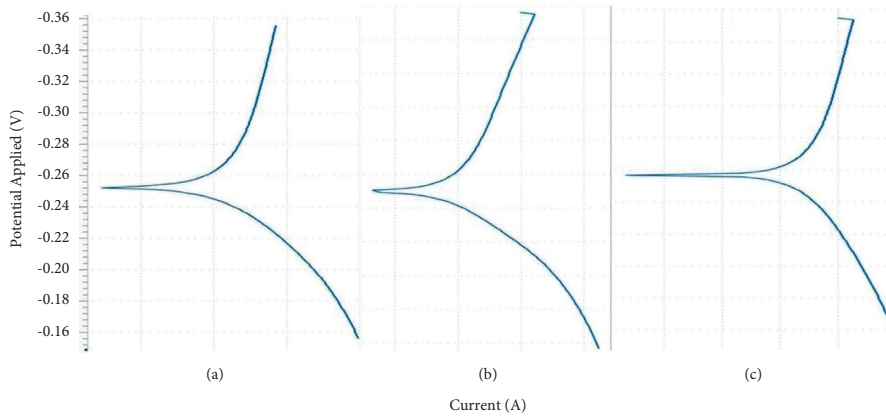


FIGURE 6: Polarization curves obtained on GrA1 steel specimen at uncoated GrA1, interface, and WC-flyash-coated GrA1 steel.

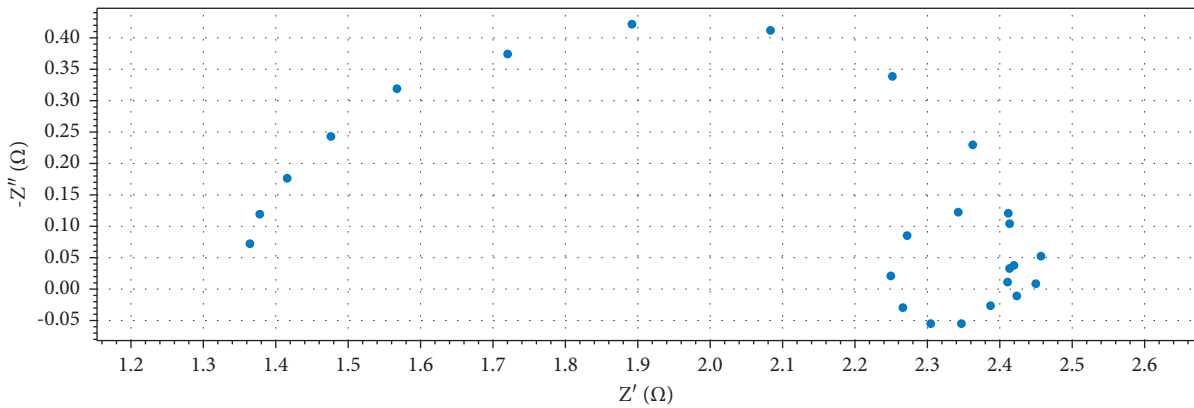
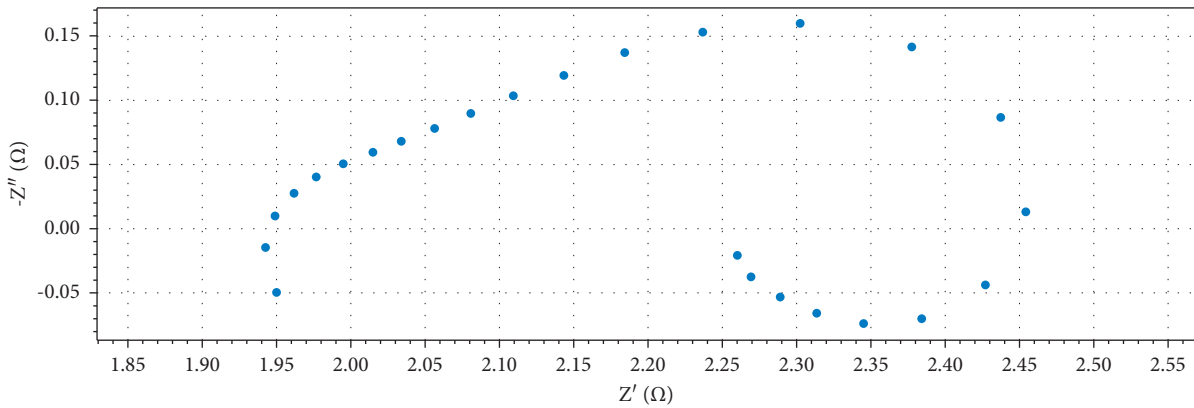
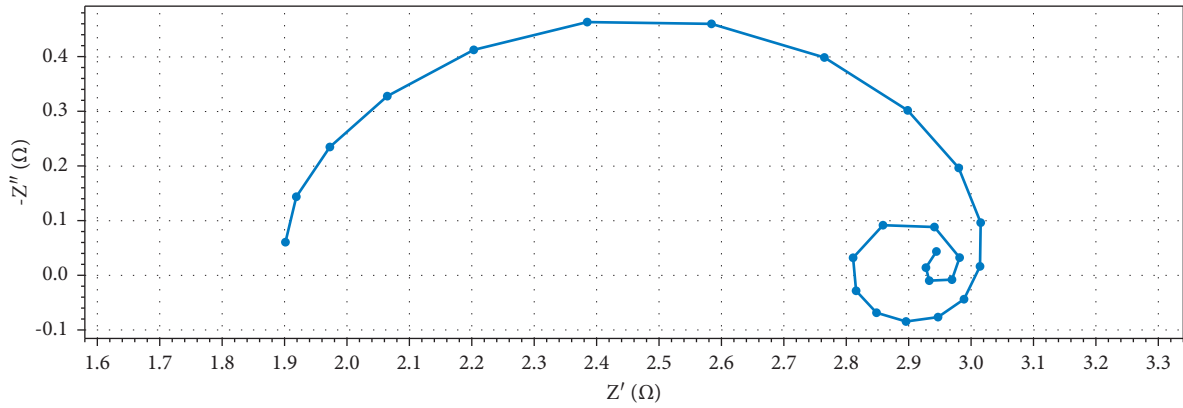
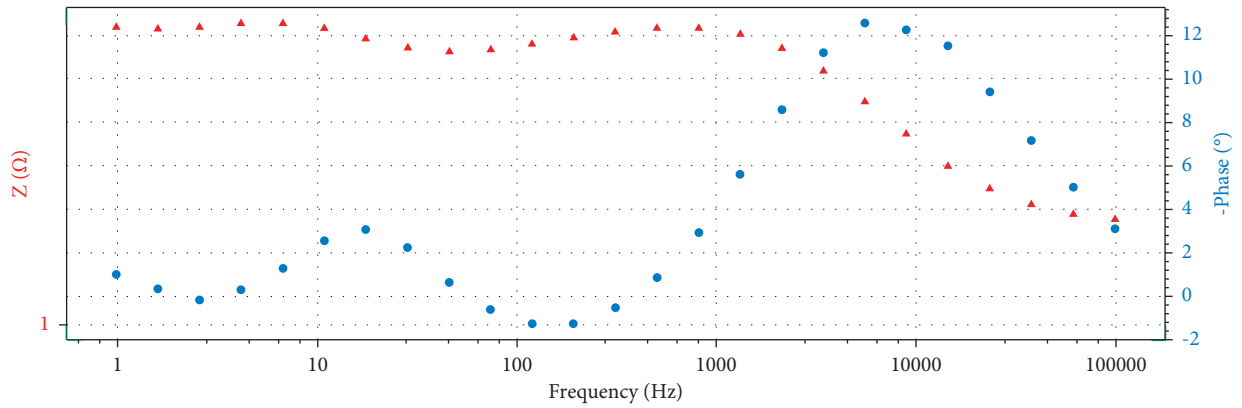


FIGURE 7: Continued.

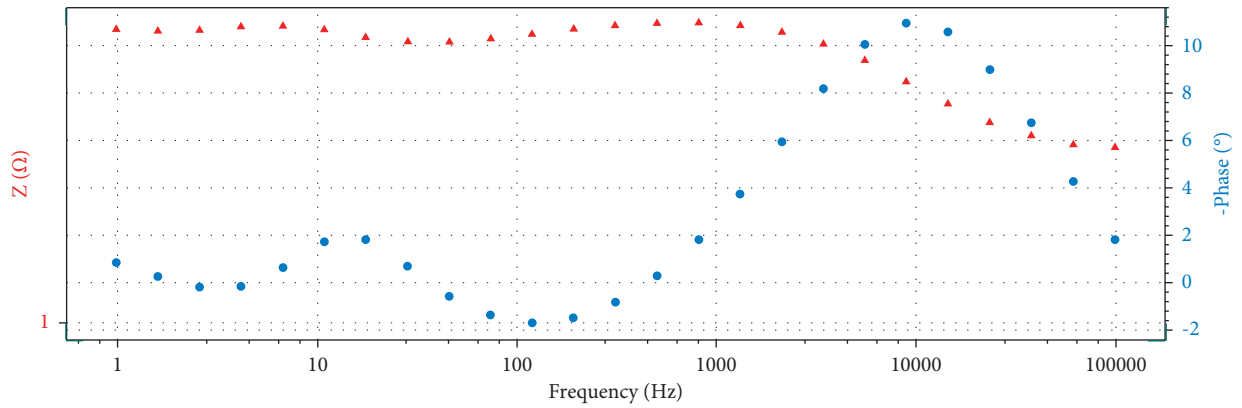


(c)

FIGURE 7: Electrochemical impedance spectra (Nyquist plot) of WC-flyash-coated GrA1 steel.



(a)



(b)

FIGURE 8: Continued.

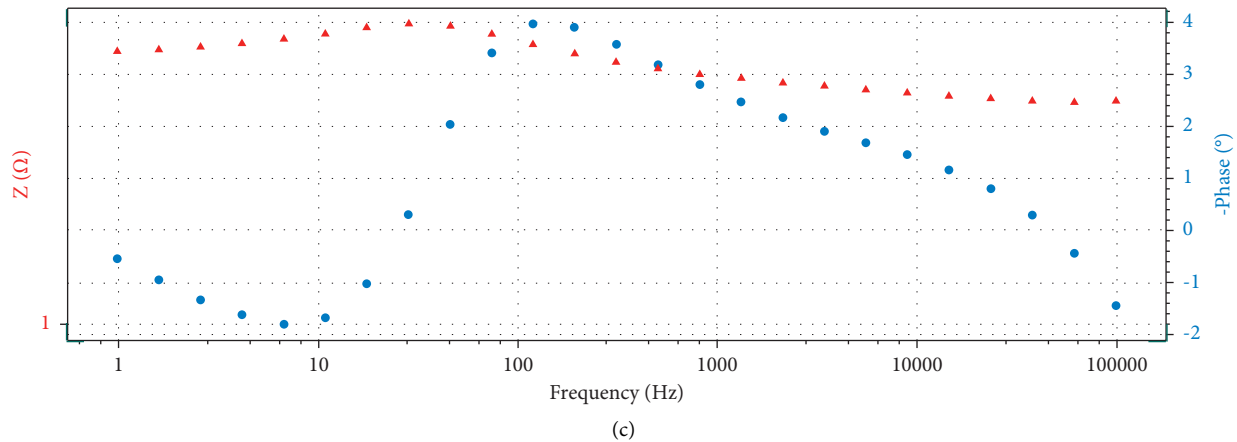


FIGURE 8: Phase angle plots of uncoated GrA1, interface, and WC-flyash-coated GrA1 steel.

#### 4. Conclusions

The curiosity of this examination was promoted through the use of cathodic assurance to kill the impacts of erosion under 3.5% NaCl climate. The HVOF splash measure gives the chance of creating WC-flyash coatings on evaporator tube steel. The uncovered substrate steel shows extreme spalling, stripping off scale and weight acquired was substantial during electrochemical consumption concentrated under the climate of 3.5% NaCl arrangement.  $\text{Fe}_2\text{O}_3$  was distinguished as the significant stage by SEM and EPMA investigation in the size of uncovered steel. The coating porosity lies between the scope of 1–3.5%, which was discovered to be helpful in creating consumption opposition in heater tube steel (GrA1). WC-flyash covering shows the least estimation of porosity and gave better protection from consumption. The arrangement of defensive oxides like  $\text{NiCr}_2\text{O}_4$ ,  $\text{NiO}$ , and  $\text{C}_2\text{O}_3$  in the scale could be added to the better consumption opposition of coatings. Spalling of scale for WC-flyash coatings was nearly less. The associated dissipation with tungsten from the scale may have ascribed to the least consumption opposition as demonstrated by 90% WC-10% flyash covering.

#### Data Availability

The data used to support the findings of this study are included within the article.

#### Disclosure

This work was performed as a part of the employment of Addis Ababa Science and Technology University, Ethiopia.

#### Conflicts of Interest

The authors declare that there are no conflicts of interest.

#### References

- [1] R. A. Rapp and Y.-S. Zhang, "Hot corrosion of materials: fundamental studies," *Journal of the Minerals Metals & Materials Society*, vol. 46, no. 12, pp. 47–55, 1994.
- [2] S. Srikanth, Z. Wang, H. Tu et al., "Functional properties of the *Drosophila melanogaster* inositol 1,4,5-trisphosphate receptor mutants," *Biophysical Journal*, vol. 86, no. 6, pp. 3634–3646, 2004.
- [3] C. I. Walker, "Slurry pump side-liner wear: comparison of some laboratory and field results," *Wear*, vol. 250, no. 1–12, pp. 81–87, 2001.
- [4] K. Sugiyama, S. Nakahama, S. Hattori, and K. Nakano, "Slurry wear and cavitation erosion of thermal-sprayed cermets," *Wear*, vol. 258, no. 5–6, pp. 768–775, 2005.
- [5] L. Pawlowski, *The Science and Engineering of Thermal Spray Coatings*, Wiley, Hoboken, NJ, USA, 2008.
- [6] M. Ivosevic, R. A. Cairncross, and R. Knight, "3D predictions of thermally sprayed polymer splats: modeling particle acceleration, heating and deformation on impact with a flat substrate," *International Journal of Heat and Mass Transfer*, vol. 49, no. 19–20, pp. 3285–3297, 2006.
- [7] G. Bolelli, L. Lusvardi, and M. Barletta, "HVOF-sprayed WC-CoCr coatings on Al alloy: effect of the coating thickness on the tribological properties," *Wear*, vol. 267, no. 5–8, pp. 944–953, 2009.
- [8] D. Chuanxian, H. Bingtang, and L. Huiling, "Plasma-sprayed wear-resistant ceramic and cermet coating materials," *Thin Solid Films*, vol. 118, no. 4, pp. 485–493, 1984.
- [9] X. Ning, C. Wiraja, D. C. S. Lio, and C. Xu, "Al dmpffscoating," *Advanced healthcare materials*, vol. 9, no. 10, Article ID 2000147, 2020.
- [10] A. Ibrahim and C. C. Berndt, "Fatigue and deformation of HVOF sprayed WC-Co coatings and hard chrome plating," *Materials Science and Engineering A*, vol. 456, no. 1–2, pp. 114–119, 2007.
- [11] T. S. Sidhu, S. Prakash, and R. D. Agrawal, "State of the a coating investigations-A review," *Marine Technology Society Journal*, vol. 39, no. 2, pp. 53–64, 2005.
- [12] E. Sadeghi and S. Joshi, "Chlorine-induced high-temperature corrosion and erosion-corrosion of HVOF and HVOF-sprayed amorphous Fe-based coatings," *Surface and Coatings Technology*, vol. 371, pp. 20–35, 2019.



- [13] B. Rad, R. Hamid, M. Daroonparvar et al., "Characterization and corrosion behavior evaluation of nanostructured TiO<sub>2</sub> and Al<sub>2</sub>O<sub>3</sub> 3-13 wt.% TiO<sub>2</sub> coatings on Aluminum alloy prepared via high-velocity oxy-fuel spray," *Journal of Materials Engineering and Performance*, vol. 30, no. 2, pp. 1356–1370, 2021.
- [14] M. Ravichandran, S. Saravanan, and V. Balasubramaniyan, "Investigations on erosion and corrosion behavior of high-velocity oxy-fuel sprayed WC-Cr<sub>3</sub>C<sub>2</sub>-Ni coatings on AISI 1018 steel," *HTM Journal of Heat Treatment and Materials*, vol. 71, no. 4, pp. 163–169, 2016.
- [15] R. J. K. Wood and J. A. Wharton, "Coatings for tribocorrosion protection," *Tribocorrosion of passive metals and coatings*, pp. 296–333, 2011.
- [16] B. E. Naveena, R. Keshavamurthy, and N. Sekhar, "Slurry erosive wear behaviour of plasma-sprayed flyash-Al<sub>2</sub>O<sub>3</sub> coatings," *Surface Engineering*, vol. 33, no. 12, pp. 925–935, 2017.
- [17] S. Matthews, M. Hyland, and B. James, "Long-term carbide development in high-velocity oxygen fuel/high-velocity air fuel Cr<sub>3</sub>C<sub>2</sub>-NiCr coatings heat treated at 900°C," *Journal of Thermal Spray Technology*, vol. 13, no. 4, pp. 526–536, 2004.
- [18] J. Vicenzi, D. L. Villanova, M. D. Lima, A. S. Takimi, C. M. Marques, and C. P. Bergmann, "HVOF-coatings against high temperature erosion (~300°C) by coal fly ash in thermoelectric power plant," *Materials & Design*, vol. 27, no. 3, pp. 236–242, 2006.
- [19] G. Singh, S. Kumar, and S. S. Sehgal, "Erosion tribo performance of HVOF deposited WC-10Co-4Cr and WC-10Co-4Cr+ 2% Y<sub>2</sub>O<sub>3</sub> micron layers on pump impeller steel," *Particulate Science & Technology*, vol. 38, no. 1, pp. 34–44, 2020.
- [20] M. R. Ramesh, S. Prakash, S. K. Nath, P. K. Sapra, and B. Venkataraman, "Solid particle erosion of HVOF sprayed WC-Co/NiCrFeSiB coatings," *Wear*, vol. 269, no. 3-4, pp. 197–205, 2010.
- [21] A. S. Praveen, J. Sarangan, S. Suresh, and B. H. Channabasappa, "Optimization and erosion wear response of NiCrSiB/WC-Co HVOF coating using Taguchi method," *Ceramics International*, vol. 42, no. 1, pp. 1094–1104, 2016.
- [22] O. Dagdag, A. Berisha, Z. Safi et al., "Highly durable macromolecular epoxy resin as anticorrosive coating material for carbon steel in 3% NaCl: computational supported experimental studies," *Journal of Applied Polymer Science*, vol. 137, no. 34, Article ID 49003, 2020.
- [23] O. Dagdag, R. Hsissou, A. El Harfi et al., "Fabrication of polymer based epoxy resin as effective anti-corrosive coating for steel: computational modeling reinforced experimental studies," *Surfaces and Interfaces*, vol. 18, Article ID 100454, 2020.
- [24] S. Kiyota, B. Valdez, M. Stoytcheva, R. Zlatev, and J. M. Bastidas, "Anticorrosion behavior of conversion coatings obtained from unbuffered cerium salts solutions on AA6061-T6," *Journal of Rare Earths*, vol. 29, no. 10, pp. 961–968, 2011.
- [25] Q. Song, R. Zhao, T. Liu et al., "One-step vapor deposition of fluorinated polycationic coating to fabricate antifouling and anti-infective textile against drug-resistant bacteria and viruses," *Chemical Engineering Journal*, vol. 418, Article ID 129368, 2021.
- [26] O. Elhaitamy, M. El Marsi, L. Lahlou et al., "Monte Carlo simulations of noble gas ion beam sputtering yield of MgO, CaO, SrO, and BaO with various thin coatings in AC-PDP cells," *Surface and Interface Analysis*, vol. 52, no. 3, pp. 84–90, 2020.
- [27] Z. A. Fazel, H. Elmkhah, A. Fattah-Alhosseini, K. Babaei, M. Meghdari, and M. Meghdari, "Comparing electrochemical behavior of applied CrN/TiN nanoscale multilayer and TiN single-layer coatings deposited by CAE-PVD method," *Journal of Asian Ceramic Societies*, vol. 8, no. 2, pp. 510–518, 2020.